Heliyon 10 (2024) e25656

Contents lists available at ScienceDirect

Heliyon

journal homepage: www.cell.com/heliyon

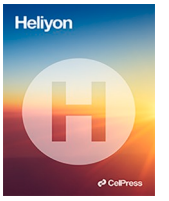

Research article

# Analysis of internal heat recovery capability in air-cooled indirect fired GAX-based absorption chiller in part-load operation

María Esther Palacios-Lorenzo *, José Daniel Marcos

*Energy Engineering Department, UNED, Juan Del Rosal 12, 28040, Madrid, Spain*

ARTICLE INFO

*Keywords:*
Part-load
Thermodynamics
Absorption
Ammonia-water
Gax
Hot climate

ABSTRACT

Single-effect absorption chillers are the most popular because of their low cost, despite their low COP. Among them, GAX-based AirCooled absorption chillers are very interesting because they have improved COP because of their ability to recover internal heat at low thermal lifts. This workshop analysed the ability of these types of chillers to recover internal heat at high thermal lifts by changing the pressure drop of an extra valve, a feature of the Robur absorption chiller when operating in subzero applications. The complete differential mathematical model analyses the components involved in heat supply and recovery and provides information on their operation. A thorough assessment of exergy destruction in the absorption refrigeration system was carried out. The main results show that when the chiller is driven at a temperature of 210 °C and an ambient temperature of 40 °C, a rise in the pressure drop of the additional valve, $\Delta P_{val1}$, from 175 to 700 kPa causes the extension of the vapour purification process to be reduced by 13.7% in the column of distillation and by 70.6% in the rectifier. Despite the adverse effect of $\Delta P_{val1}$ increase on the cooling capacity, there is no risk that the distillation column operates in weeping mode. However, this adjustment increases the internal thermal load of the generator by 26.9%. Furthermore, the mass fraction of the refrigerant flow is very similar. In addition, the occurrence of a two-phase solution flow at the input of a solution cooling absorber is the practical upper limit of $\Delta P_{val1}$. The refrigerant flow in the solution cooling absorber is reduced by 21.3%. Finally, the contribution of the heat recovery loop to the total exergy destruction in the refrigeration system rises slightly by 2.7% when $\Delta P_{val1}$ increases due to the contribution of the vapour purification system, which increases at the expense of that of the re-boiler and the SolutionCooled absorber. The results of this study show to what extent the modified GAX-based cycle can function effectively at high thermal lifts.

## 1. Introduction

Today, it is essential to reduce dependence on fossil fuels to reduce the effects of global warming [1]. The refrigeration industry accounts for approximately 20% of global electricity consumption and 7.8% of global greenhouse gas emissions [2]. In this context, thermal refrigeration systems, in general, and absorption chillers in particular, could help mitigate the environmental impact of the refrigeration industry. The absorption chiller is characterised by its main energy saving capacity, driven by solar energy and waste heat, and uses an environmentally friendly working fluid. In addition, due to low energy consumption, the summer electricity

* Corresponding author.
*E-mail address:* epalacios@ind.uned.es (M.E. Palacios-Lorenzo).

https://doi.org/10.1016/j.heliyon.2024.e25656
Received 20 September 2023; Received in revised form 3 January 2024; Accepted 31 January 2024
Available online 5 February 2024

requirements can be reduced [3]. Some configurations were studied to achieve high COP. The single-effect configuration requires a minimal number of components, resulting in cost reduction. Furthermore, it can be operated at a low generator temperature. As a result, the single effect configuration is the most commercially available configuration despite the lowest COP [4], leading to a high thermal rejection factor (receivable heat to-cooling capacity ratio). This is why the internal heat recovery of the cooling absorption system is improved [5].

Ammonia water is widely used under subzero conditions because it can operate at low evaporation temperatures. Furthermore, no crystallisation or vacuum problems are present. However, the vapour pressure of water in the generation process is significant in comparison to the ammonia vapour pressure. Consequently, a vapour purification process is required to remove the remaining water from the generated vapour. The purification system complicates the design of the refrigeration system and increases the loss. Several attempts have been made to eliminate the need for the purification process by replacing the ammonia-water pairs, thus enlarging the temperature difference at which the refrigerant and the absorbent boil. The most popular binary ammonia salt solutions for rectifier elimination include $NH_3$–NaSCN and $NH_3$–$LiNO_3$. However, these pairs are not without shortcomings. Therefore, the $NH_3$–NaSCN pairs have a high ammonia solubility and do not cause steel corrosion but can crystallise at low evaporation temperatures. However, the high viscosity of salt solutions limits the performance of the $NH_3$–$LiNO_3$ cooling system [6]. The key role of the purification system in the performance of ammonia water refrigeration systems has been extensively studied [7,8]. In AirCooled ammonia-water absorber refrigeration systems, the ammonia vapour purification process becomes more important as the ambient temperature increases. With high-efficiency stripping sections, the design of the column of distillation can be simplified by eliminating the rectifying section [9]. In addition to the ammonia vapour purification system, other subcomponents are added to the basic single-effect ammonia water absorption cycle to improve its performance. These include solution heat exchangers and refrigeration heat exchangers, which increase COP by 44 % and 8 %, respectively, and enable internal energy recovery [10]. Reorganisation of the cycle streamlines optimises internal heat recovery and improves the overall performance of the system. Thus, the GAX-based absorption cycle enables some absorption heat to be recovered internally by the generator [11], especially when the thermal lift (the temperature difference between condensation and evaporation) is low [12]. Velázquez et al. [13] propose a methodological analysis of an AirCooled absorption system for air conditioning purposes, which does not include the recovery of heat from the economiser and the recovery of heat from rectification. Gomez et al. [14] reported the experimental evaluation of a GAX-based cycle for air conditioning purposes. Saghiruddin et al. [15] carried out an economic analysis using a heat recovery absorber, reporting an increase of 20–30% in the performance of an ammonia water chiller, in addition to a 25% reduction in energy cost. Du et al. [16] examined the internal heat recovery capacity of ammonia in a complete condensation water absorption system. They found that the best improvement is achieved when there is a temperature overlap between the absorption and generating processes. According to Dai et al. [17], the size of the SolutionCooled absorber heat exchanger has the greatest impact on the cycle. Jawahar et al. [18] carried out an analysis on a real AirCooled direct-fired ammonia-water modified GAX absorption chiller. They increased the total internal heat recovered by 30–40%, resulting in an improvement in the efficiency of the machine.

The GAX-based cycle can achieve internal heat recovery due to the partial temperature overlap between the generator and the absorber, which can be reduced when the cooling system operates outside the design conditions. Therefore, the key question is how it performs under partial loads, especially under high thermal lifts. Aprile et al. [19] conducted experimental research on GAX heat pumps to improve the performance of the system under partial load by controlling the generator flow. On the other hand, AirCooled ammonia water absorption chillers for refrigerant purposes have the disadvantage of high thermal lifts in addition to the low thermal conductance of heat rejection by air cooling, increasing the size of the chiller [20].

The purpose of the study is to analyse the commercial indirect AirCooled single-effect $NH_3/H_2O$ absorption chiller, specifically the Robur refrigerant absorption machine (ACF60-00 LB), which operates with hot water for subzero conditions in the dairy sector. This chiller operates on a modified GAX-based cycle, incorporating an additional valve, which enables the active control of the pressure levels of the chiller in part-load operation and, therefore, reduces the chiller size. The present work aims to evaluate the ability of the modified GAX-based cycle implemented in the Robur chiller to recover internal heat during part load operation, under this strategy, particularly at high thermal lifts.

For this purpose, a comprehensive differential mathematical model is developed. The model uses the Colburn and Drew equations and includes heat and mass transfer coefficients evaluated locally. The accuracy of the model was validated using both manufacturer-provided experimental data and data from the literature. Furthermore, the study introduces a novel approach to exergy analysis reported by Blanco-Marigorta and Marcos [21] by implementing the concept of dead state, leading to a more thorough evaluation of exergy destruction in the system.

The main objective of this research study is to analyse the ability of the refrigeration system to recover internal heat to improve its overall performance at high thermal lift. In particular, the findings show to what extent the modified GAX-based cycle can operate effectively at high thermal lifts. As a result, an increase in the internal thermal load of the generator assembly is observed, specifically within the solution heat exchanger and the column of distillation. Additionally, there is a potential risk of two-phase flow at the inlet of the SolutionCooled absorber. However, the contribution of the internal heat recovery system to the total exergy destruction in the refrigeration system is not particularly significant.

## 2. Methodology

### 2.1. System description

Fig. 1 shows a scheme of the chiller, whose structure is outlined in Table 1. The chiller comprises an evaporator, condenser,

SolutionCooled absorber, AirCooled absorber, and generator. The purification system includes a column of distillation and a SolutionCooled rectifier located at the top, which is responsible for achieving a high-purity vapour. The condenser, AirCooled absorber, and re-boiler are equipped with annular fins. The evaporator is constructed as a shell-and-tube heat exchanger with baffles. The SolutionCooled absorber and SolutionCooled rectifier consist of helical tubes, each differing in the numbers of turns, denoted as, $N_{turns}$.

The design of each tray of the column of distillation is determined defined by various parameters such as inner diameter $D_i$, hole diameter, $d_h = 0{,}00381$ m, tray thickness, $e_{tray}$, tray spacing, $S_t$, weir length, $l_w$, hole pitch, $s_h = 3\ d_h$, weir height, $h_w$, as well as two relationships, $A_h/A_a = f_2(d_h/s_h)$ and $A_d/A_t = f_1(l_w/D_i)$ [22], where $A_d$, $A_t = \pi/4\ D_i^2$, and $A_a = A_t$ - $2A_d$, respectively representing the downcomer area, the area of the column, and the active area. The efficiency of the refrigeration heat exchanger has been set to 0.9. To limit temperature glide, the refrigerant quality has been set to 0.96 at the evaporator outlet. The generator heat recovery system comprises the solution heat exchanger and the distillation column heat exchanger. The chiller comprises three valves: the solution valve, refrigerant valve, and valve 1 - the latter enables the regulation of the high pressure level.

### 2.2. Mathematical model

The Engineering Equation Solver software has been used to implement a differential mathematical code for a modular-form. Each module characterizes the performance of a fundamental system within Robur® absorption refrigeration by employing physical equations derived from the principles of mass, species, and energy balance.

$$\sum_i \dot{m}_{in} - \sum_i \dot{m}_{out} = 0 \tag{1}$$

$$\sum_i (x \bullet \dot{m})_{in} - \sum_i (x \bullet \dot{m})_{out} = 0 \tag{2}$$

$$\sum_i (h \bullet \dot{m})_{in} - \sum_i (h \bullet \dot{m})_{out} + \dot{Q}_i = 0 \tag{3}$$

x, $\dot{m}$ and $h$ denotes the mass fraction, mass flowrate and enthalpy of the flow. Heat transferred across the $i$-finite volume, $\dot{Q}_i$, is evaluated by the Newton's law of cooling:

$$\dot{Q}_i = h_t A_i \frac{(T_i - T_w) - (T_{i+1} - T_w)}{ln\left(\frac{T_i - T_w}{T_{i+1} - T_w}\right)} \tag{4}$$

in which, $h_t$ represents the heat transfer coefficient evaluated locally, and $A_i$ signifies the heat transfer surface of the finite volume, $i$. The thermodynamic property database for working fluids is sourced from Ibrahim et al. [23]. Throughout all operational scenarios, the pump solution's flow rate remains constant [24]. The cooling speed facing the air remains unaltered. The model considers the fluctuation of thermal conductivity concerning temperature and loading conditions [25]. The analysis is based on the following assumptions:

- Processes are stationary.

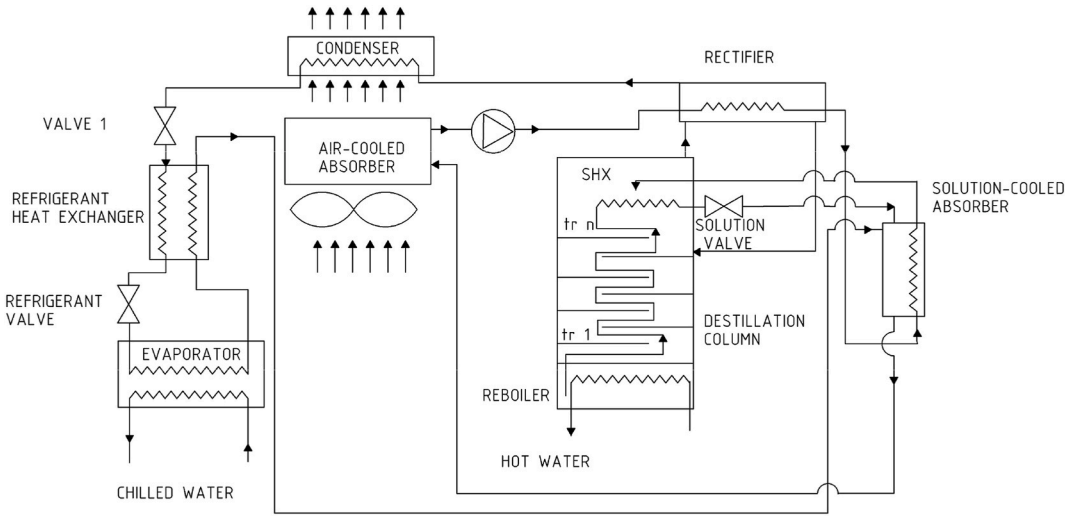


**Fig. 1.** Scheme of the refrigerant absorption machine (ROBUR ACF60-00 LB).

**Table 1**
Chiller geometry.

| Condenser & AirCooled absorber | | Evaporator | | Rectifier & SolutionCooled absorber | | Re-boiler | | Column of distillation | |
|---|---|---|---|---|---|---|---|---|---|
| $D_i$ [m] | 0,02 | $D_i$ [m] | 0.015 | $D_{to}$ [m] | 0,075 | $h_f$ [m] | 0,63 | $D_i$ [m] | 0,075 |
| $s$ [m] | 0,003 | $s$ [m] | $1{,}15(D_i + e)$ | $D_{wi}$ [m] | 0,0065 | $s$ [m] | 0,003 | $S_t$ [m] | 0,15 |
| $t_m$ [m] | 0,0002 | $e$ [m] | 0.002 | $D_{ti}$ [m] | 0,045 | $t_m$ [m] | 0,0004 | $A_d$ [$m^2$] | 0,12 $A_t$ |
| e [m] | 0.002 | $N_{tube}$ | 35 | $e$ [m] | 0,002 | | | $e_{tray}$ [m] | 0,003 |
| $N_{tube}$ | 2 | $L$ [ m] | 1,1 | $N_{turns\ cabs}$ | 15 | | | $h_w$ [m] | 0,1 $S_t$ |
| | | $D_{i,shell}$ [m] | $(N_{tube} + 1)\ s$ | $N_{turns\ rect}$ | 40 | | | $A_h/A_a$ | $f_2(d_h/s_h)$ |
| | | | | | | | | $A_d/A_t$ | $f_1(l_w/D_i)$ |

- The frictional pressure drop in the components is neglected, except for the valves.
- The solution flow that comes out the re-boiler is in a saturated state.
- The refrigerant exiting the evaporator and the condenser is in a saturated state.
- The refrigerant heat exchanger's effectiveness is constant.
- Heat losses to the surroundings are disregarded.
- The flow is unidimensional.
- Mass and hear transfer take place radially within the tube.

The characteristics of each module are detailed below.

### 2.2.1. Distillation column system

The column of distillation is segmented into trays, including the SolutionCooled rectifier and the re-boiler, which are considered as additional trays. This assessment focusses on evaluating the heat flux involved in the vapour generation in the re-boiler and in the partial condensation within the rectifier. The Murphree efficiency for a vapour plate, $e_M$, calculated using the expression from Wilke-Chang [22], is employed to determine the ammonia molar fraction of the vapour coming out the $i$-tray. Consequently, the ammonia molar fraction of the vapour that comes from each i-tray, denoted as $\overline{x}_{v,i}$, can be expressed as follows,

$$\overline{x}_{v,i} = \overline{x}_{v,i-1} \bullet (1 - e_M) + e_M \overline{x}_{v\ e,i}, \tag{5}$$

where $\overline{x}_{v\ e,i}$ represents the molar mass fraction of the vapour exiting the i-tray under thermodynamic equilibrium conditions. The influence of fluid entrainment is assessed using the Fair approach [22]. To simplify, any exchange between the vapour flow and the liquid from the re-boiler is omitted. Equations (1)–(5) govern the concurrent mass and heat transfer processes occurring in each tray within the column of distillation.

### 2.2.2. Condenser and evaporator systems

The condenser and evaporator are divided into finite volumes, encompassing both the refrigeration and coolant sides. To accurately determinate the heat transfer coefficient ($h_{t\ ref}$) on the refrigeration side, specifically for an ammonia-water mixture, which is a zeotropic refrigerant mix, the Silver-Bell-Ghaly method is utilized.

**Table 2**
Heat and mass transfer coefficients.

| Device | | Regime | Heat transfer coefficient | Mass transfer coefficient |
|---|---|---|---|---|
| Re-boiler | Solution side | – | Gorenflo [37] & Taboas et al. [38] | |
| Evaporator | | | Klimenko [37] &Taboas et al. [38] | |
| Absorbers & rectifier | Liquid to tube surface (condensation theory in horizontal tube) | laminar | Nusselt eq. smooth film [39] waviness: Kutateladze & Gogonin [39] | – |
| | | turbulent | Yüksel & Müller [40] shear stress: Numrich [39] | – |
| Evaporator & re-boiler | Coupling fluid side | – | VDI Wärmeatlas [39] | – |
| Rectifier & SolutionCooled absorber | | | Mills [37] | |
| AirCooled absorber & Condenser | | | Qasem et al. [40] | |
| Absorbers & rectifier | Vapour to interface | – | Gnielinski [39] | Chilton & Colburn analogy [39] |
| Rectifier & SolutionCooled absorber | Liquid to interface | – | Film condensation theory (horizontal tube) [40] | Chilton & Colburn analogy [39] |
| AirCooled Absorber | Liquid to interface | intermittent stratified bubble | Film condensation theory (horizontal tube) [40] | Scott & Hayduk [41] Scott & Hayduk [41] Ciborowski & Rychlicki [42] |

$$h_{t,ref} = h_{t,pure} / (1 + K)^4 \tag{6}$$

where $h_{t,pure}$ denotes the heat transfer coefficient, calculated based on the model for the pure fluid using mixture properties (refer to Table 2). $K$ refers to a correction factor, assessed by Taboas et al. [26]. The set of non-linear Equations (1)–(4) and (6) constitutes the mathematical model of the evaporator and the condenser.

### 2.2.3. Re-boiler system

The re-boiler module considers only a single control volume that encompasses the hot water and the solution side to calculate the transferred heat flux. Like the evaporator and condenser modules, the Silver-Bell-Ghaly method allows the evaluation of the heat transfer coefficient (see Table 2). Nonlinear Equations (1)–(4) and (6) form the mathematical model of the re-boiler.

### 2.2.4. Rectifier, SolutionCooled absorber and AirCooled absorber systems

Each device is discretised in finite volumes, including four distinct zones: the coolant side, the vapour-liquid interface, the liquid solution side and the vapour side. The mass continuity at the interface was carried out to evaluate the total molar flow from the vapour flow to the interface, $\dot{n}$.

$$\dot{n}_{NH_3 v} = \dot{n}_{NH_3 L} = \dot{n} \bullet z \tag{7}$$

where $\dot{n}_{NH_3 v}$ refers to the molar flux of ammonia from the vapour flow to the interface, $\dot{n}_{NH_3 L}$ denotes the molar flux of ammonia from the interface to the liquid flow. The ammonia molar fluxes are given by Bird expression [27].

$$\dot{n}_{NH_3 v} = h_{m,v} \bullet z \bullet ln\left(\frac{z - \overline{x}_{vi}}{z - \overline{x}_v}\right) \tag{8}$$

$$\dot{n}_{NH_3 L} = h_{m,Li} \bullet z \bullet ln\left(\frac{z - \overline{x}_L}{z - \overline{x}_{Li}}\right) \tag{9}$$

where $h_{t,v}$ is the vapour mass transfer coefficient, $z$ is the ammonia to total molar flux ratio, $\overline{x}_v$ is the ammonia molar mass fraction of the vapour. The ammonia mass transfer is defined as the transfer from the vapour flow to the liquid flow. Subscript $i$ indicates thermodynamic equilibrium. Accordingly, the ammonia flux, $\dot{n}_{NH_3}$, and the total mass flux, $\dot{m}$, are evaluated as

$$\dot{m}_{NH_3} = \dot{n}_{NH_3} \bullet PM_{NH_3} \tag{10}$$

$$\dot{m} = \dot{n}_{NH_3} \bullet PM_{NH_3} + \dot{n} \bullet (1 - z) \bullet PM_{H_2O} \tag{11}$$

here PM refers to the molecular weight. The coupling between heat transfer and mass transfer at the interface is expressed by the energy continuity at the interface.

$$q_L = q_v + \dot{m}_{NH_3} \Delta\widetilde{h}_{NH_3} + \dot{m}_{H_2O} \Delta\widetilde{h}_{H_2O} \tag{12}$$

being $q$ the heat flux. $\Delta\widetilde{h}$ refers to the partial enthalpies difference of the liquid and vapour components at the interface. Non-linear Equations (1)–(4) and (7)–(12) dictate the interdependent mass and heat transfer processes occurring in each finite volume that includes the AirCooled and SolutionCooled absorbers and the rectifier.

### 2.2.5. Evaluation of irreversibilities

Exergy destruction was assessed by conducting an exergy balance that segregates the total exergy ($e_i$) into its chemical and physical constituents. The physical component is evaluated as

$$e_i^{PH} = h_i - h_{i,0} - T_0 (s_i - s_{i,0})$$

The base point (0) for determining physical exergy is related to the pressure inside the refrigeration absorption system when it is inactive, $P_0$ [21], and the ambient reference temperature of T0 = 25 °C. The chemical component is calculated as [28].

$$e_i^{CH} = x_i \bullet e_{NH3}^{CH} + (1 - x_i) \bullet e_{H2O}^{CH} + w_{xi}^{mix}$$

where $w_{xi}^{mix}$ represents the specific work linked with the mixture consisting of pure refrigerant (ammonia) and pure absorber (water).

$$w_{xi}^{mix} = \left[h_{j0} - x_i \bullet h_{NH3,0} - (1 - x_i) \bullet h_{H2O,0}\right] - T_0 \left[s_{j0} - x_i \bullet s_{NH3,0} - (1 - x_i) \bullet s_{H2O,0}\right]$$

The specific exergy values for an absorption refrigeration system are assumed as follows: $e_{H2O}^{CH} = 45$ kJ kmol$^{-1}$ and $e_{NH3}^{CH} = 336\,684$ kJ kmol$^{-1}$.

### 2.2.6. Evaluation of heat and mass transfer coefficients

The model designed for the chiller system considers flow patterns in the AirCooled absorber [29]. In the intermittent regime, void

fraction [30–33], velocity of the bubble present in the slug [34], and bubble length [35] have been evaluated. To calculate the void fraction in the stratified regime, the correlation of Armand-Massina [36] is applied. In addition, a variety of correlations and approaches are used to evaluate the heat transfer and mass transfer coefficients for all components. Table 2 provides a comprehensive summary of these coefficients.

### 2.3. Solution method

An iterative method has been employed to fuse all the apparatus that makes up the absorption chiller. A simplified model flow chart is illustrated in Fig. 2. In the initial phase, certain parameters, denoted as 0 in Fig. 2, are assumed, and subsequently iteratively refined through species, mass, and energy balance, involving heat and mass transfer coefficients. Key variables such as the low-pressure level

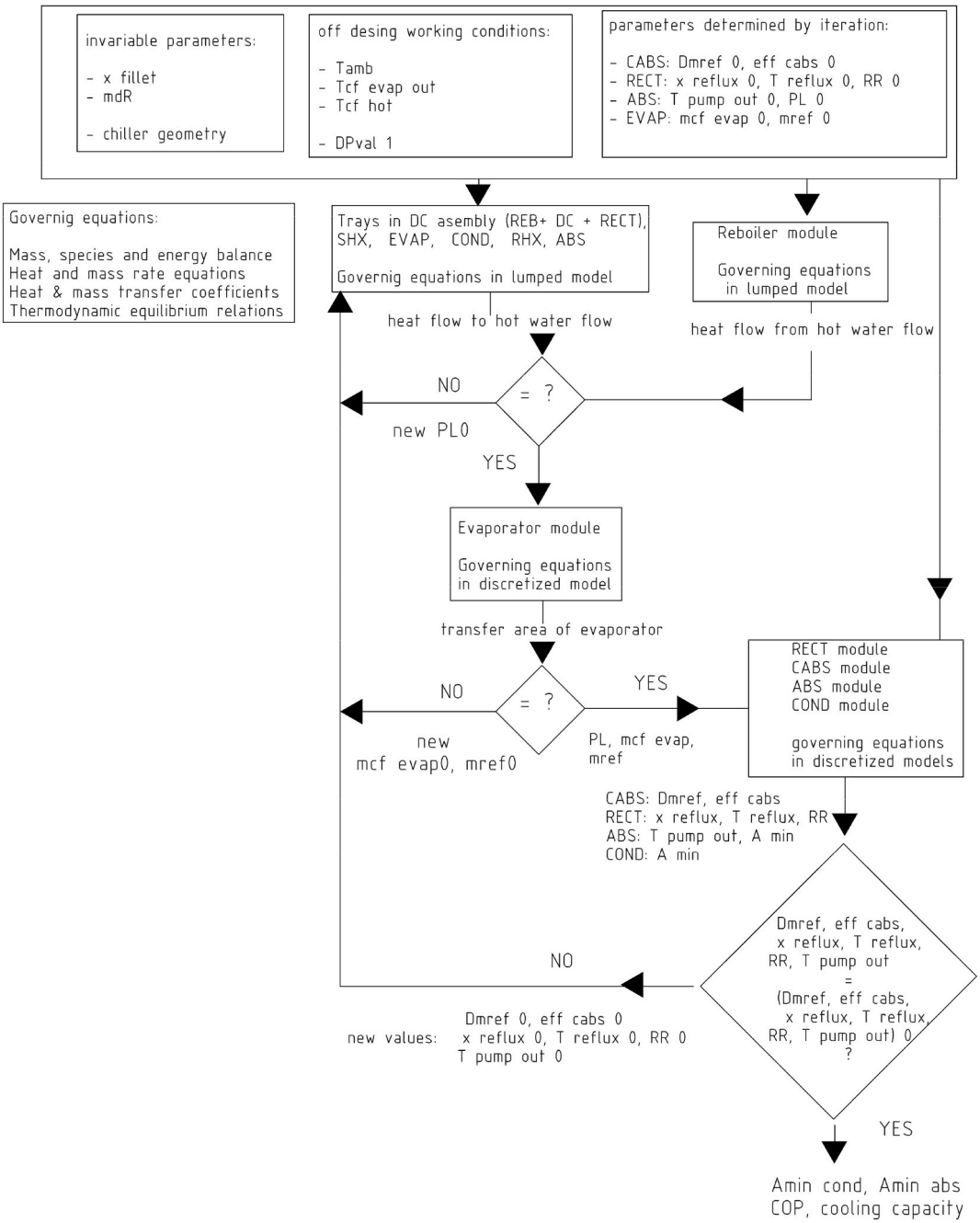


**Fig. 2.** Simplified model flow chart.

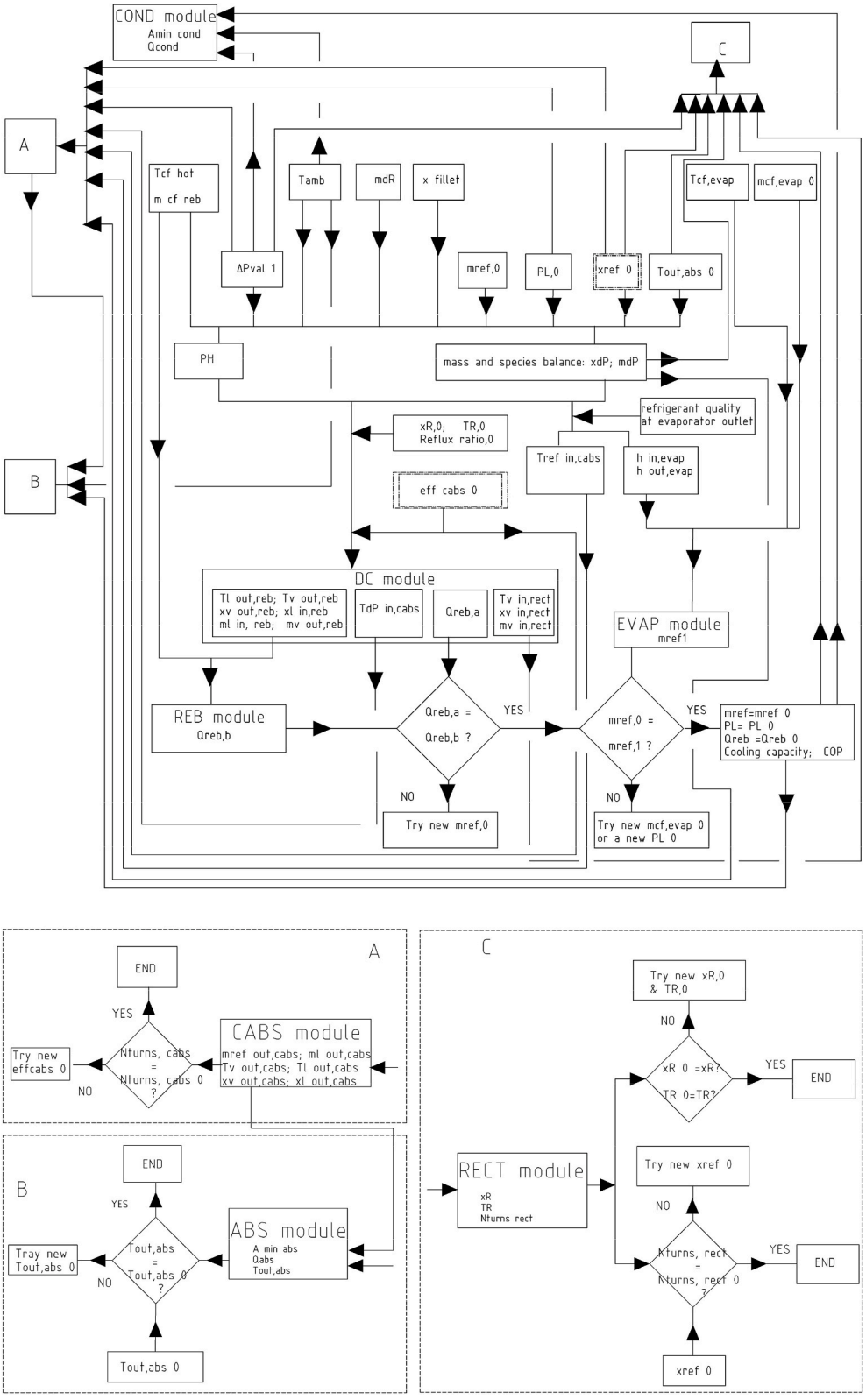


**Fig. 3.** Calculation flow chart.

($P_L$), the flow rate of chilled water, $\dot{m}_{cf,evap}$, and the heat flow of the hot water, $\dot{m}_{cf,reb}$, have been evaluated by aligning the heat flow of the hot water $\dot{m}_{cf,reb}$, with that to the solution at the re-boiler. Before this, a check is made to verify that the evaporator can complete the evaporation process.

Fig. 3 illustrates the calculation flow chart. The chilled water mass flow rate, $\dot{m}_{cf,evap}$, is considered as a variable magnitude. This is consistent with the data from manufacturer, which indicate a particular interval of change. The calculation procedure is summarised below. For all operation conditions of the system (fixed by $T_{amb}$, $T_{cf\,h,}$ and $\dot{m}_{cf,reb}$), $\Delta P_{valv\ 1}$ is set. The physical validity of the solution is ensured by imposing the corresponding geometric constraints.

1. Make an initial estimation of the low pressure level, $P_L$, the mass fraction of refrigerant, $x_{ref}$, the solution temperature at the pump outlet, $T_{pump\ out}$, the refrigerant mass flow rate $\dot{m}_{ref}$, the SolutionCooled absorber effectiveness, $\varepsilon_{cabs}$, the reflux ratio, $RR$, the temperature of the condensate and the mass fraction at the rectifier output, $T_R$ and $x_R$.
2. Execute the main module of the implemented model. This will calculate the re-boiler heat flow, $\dot{Q}_{reb}$, the mass flow rate of absorbed refrigerant in the SolutionCooled absorber, $\Delta\ \dot{m}_{ref,cabs}$, the high-pressure level ($P_H$), and the re-boiler heat flux.
3. Execute the module of the re-boiler system. Verify $\dot{Q}_{reb}$. Proceed to Step 4 if verified. Otherwise, make a new estimation of $\dot{m}_{ref}$ and return to Step 2.
4. Execute the module of the evaporator system. Verify the refrigerant mass flow rate at the evaporator exit, $\dot{m}_{cf,evap}$. Proceed to Step 5 if verified, go. On the contrary, make another estimation of $\dot{m}_{cf,evap}$, or of $P_L$, and proceed to Step 2.
5. Execute the module of the rectifier system. Verify $RR$, $T_{R,}$ $xR,$ and $N_{turns\ rect}$. Proceed to Step 6 if verified. Otherwise, make a new estimation of $RR$, $T_R$, $x_R$, and proceed to Step 2.
6. Execute the module of the SolutionCooled absorber system. Review $\varepsilon_{cabs}$ and $N_{turns,\ cabs}$. Proceed to Step 7 if verified. On the contrary, make another estimation of $\varepsilon_{cabs}$. Then proceed to Step 2.
7. Execute the module of the AirCooled absorber system. Verify $T_{pump\ out}$. Proceed to Step 8 if verified. On the contrary, make another estimation of $T_{pump\ out}$ and proceed to Step 2.

### 2.4. Model validation

The methodology was validated by assessing the coefficient of performance (COP) and cooling capacity of the AirCooled, indirect-fired ammonia-water ROBUR refrigeration absorption machine (ACF60-00 LB), provided by the manufacturer. The chiller was tested for outdoor temperatures changing from 15 to 40 °C and feed water temperatures within the range of 160–210 °C while producing chilled water at −5 °C. Details on the pressure drop in valve 1 are provided in Ref. [43], with additional information on high and low pressure levels, for an AirCooled indirect ROBUR absorption chiller operating to provide air conditioning. Lazzarin et al. [24] present more experimental data for high and low pressure levels for a direct AirCooled ROBUR chiller operating for refrigeration. Subsequently, after examining the data from Refs. [43,44], a disparity in $P_L$ and $P_H$ is evident in Figs. 4b and 5b. The discrepancy in $P_L$ arises from the operation for air conditioning purposes, and the $P_H$ results from the downsizing of the chiller. The Robur chiller includes an additional valve (referred to as valve 1 in Fig. 2). The mathematical model provides the pressure loss at valve 1 when $T_{cf\ hot} = 210$ °C, that is, $\Delta P_{valv1L} = f(T_{amb}, T_{cf\ hot} = 210$ °C). As a result, this model allows us to calibrate $\Delta P_{valv1}$ at $T_{cf\ hot} = 210$ °C using the manufacturer's data on cooling capacity and COP when the ambient temperature varies between 15 and 40 °C. Furthermore, Figs. 4a and 5a illustrate that the model aligns well with the manufacturer's data, when $\Delta P_{valv1}$ is set at $\Delta P_{valv1L}$ when $T_{cf\ hot} = 210$ °C, while it is set according to Ref. [43] when $T_{cf\ hot} = 160$ °C. Table 3 summarises the highest level of uncertainty in the model for COP, cooling capacity, and high and low pressure levels. These observations were made under specific working conditions, where $T_{amb}$ ranged from 15 to 40 °C, while $T_{cf,\ hot,}$ was set at the minimum and maximum values provided by the manufacturer, which were 160 and 210 °C, respectively.

## 3. Results

Next, the effect of $\Delta P_{valv1L}$ on the ability to recover internal heat for the refrigeration system is analysed. Exergy destruction is also evaluated. With this objective, two configurations are defined and analysed. The first, the reference configuration, is established with

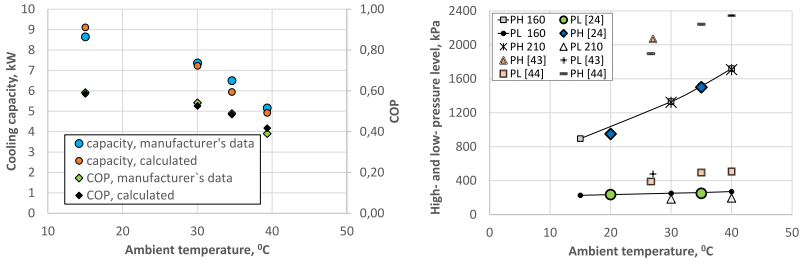


**Fig. 4.** a) Cooling capacity & COP, b) high and low pressure levels. $\Delta P_{valv1} = 175$ kPa, $T_{cf,hot} = 160$ °C.

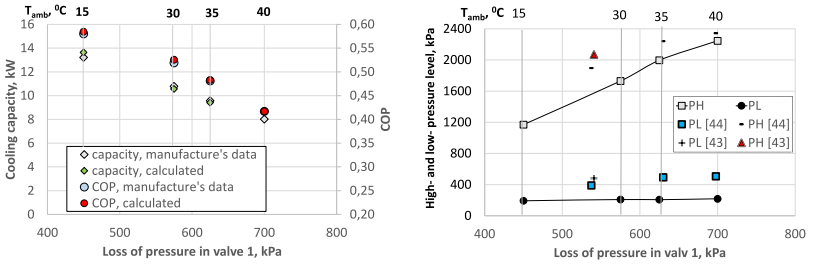


**Fig. 5.** a) Cooling capacity & COP, b) high and low pressure levels. $\Delta P_{valv1} = \Delta P_{valv1L}$, $T_{cf,hot} = 210$ °C.

**Table 3**
Validation of the model.

| | Source | Max. uncertainty, % |
|---|---|---|
| COP | Manufacture's data | 6.5 |
| Cooling capacity | Manufacture's data | 8.6 |
| High pressure level | [24] | 4.7 |
| Low pressure level | [24] | 0.5 |

$\Delta P_{valv1}$ fixed at 175 kPa, as reported in Ref. [43], and $T_{cf,hot}$ at 160 °C. The second, the personalised configuration, is defined with $T_{cf\ hot} = 210$ °C and $\Delta P_{valv1}$ set at $\Delta P_{valv1L}$. The behaviour of the main components involved in internal heat recovery is analysed when operating in each configuration, and the $T_{amb}$ ranges from 15 to 40 °C.

### 3.1. Re-boiler

Table 4 illustrates a 29.6% decrease in the thermal conductance of the re-boiler, $UA_{reb}$, with a 75% increase in $\Delta P_{val\ 1}$ at $T_{amb} = 40$ °C and $T_{cf,hot} = 210$ °C. This is attributed to the rise in the high pressure level, $P_H$. Furthermore, the effectiveness of the re-boiler, reb, improves by 7.1% due to the zeotropic character of the working solution. The combined influence of $P_H$ and $\varepsilon_{reb}$ leads to an 8.4% decrease in heat flux, $q_{reb}$. Furthermore, Table 4 indicates that increasing the temperature of the feed water, $T_{ch\ hot}$, has a contrary impact on $UA_{reb}$ and on $\varepsilon_{reb}$, followed by the re-boiler heat flux, $q_{reb}$. Consequently, $q_{reb}$ decreases by 8.4% with a 50 °C increase in $T_{ch\ hot}$. However, Fig. 6a shows that $q_{reb}$ decreases with increasing $T_{amb}$, mainly due to the reduction in $UA_{reb}$. It should be noted that $T_{amb}$ has a negligible effect on $\varepsilon_{reb}$.

Based on the analysis of the effect of each parameter on the re-boiler, including $\Delta P_{val1}$, $T_{cf,hot}$, and $T_{amb}$, it can be concluded that the increase in $q_{reb}$ in the personalised configuration (Fig. 6b) is due to the increase in $UA_{reb}$ with $T_{cf,hot}$. Note that this increase is partly offset by the increase in $\Delta P_{val\ 1}$, especially at high $T_{amb}$, where the increase in $\Delta P_{val1}$ is more pronounced. Therefore, it is advised to improve the design of the finned re-boiler surface to decrease the thermal resistance on the hot water side. This will help alleviate the adverse effects of an increase in $\Delta P_{val1}$ on the supplied heat flow.

### 3.2. Vapour purification

Vapour purification takes place mainly in the column of distillation. However, a rectifier located at the top of the column is necessary to obtain the required ammonia purity of the refrigerant flow. The performance of the column of distillation has been evaluated using the $OP_{dc}$ parameter, defined as

$$OP_{dc} = \frac{\dot{m}_{v\ out,dc} - \dot{m}_{v\ weeping}}{\dot{m}_{v\ flooding} - \dot{m}_{v\ weeping}},$$

where $\dot{m}_{v\ out,dc}$ is the vapour flow at the column of distillation outlet and $\dot{m}_{v\ flooding}$, $\dot{m}_{v\ weeping}$ is the vapour flow at flooding and weeping, respectively. Another parameter of interest is the reflux ratio, $RR_{dc}$, defined as

**Table 4**
Re-boiler. Comparative results, expressed in %.

| $\Delta P_{val\ 1}$, kPa | $T_{cf,hot}$, °C | $T_{amb}$, °C | $\Delta UA_{reb}$ | $\varepsilon_{reb}$ | $\Delta q_{reb}$ |
|---|---|---|---|---|---|
| $\Delta P_{val\ 1L}$ vs. 175 | 210 | 30 | −4.6 | 12.8 | −9.8 |
| | | 40 | −29.6 | 7.1 | −8.4 |
| 175 | 210 vs. 160 | 30 | 14.7 | −24.1 | 47.5 |
| | | 40 | 24.8 | −13.7 | 53.4 |

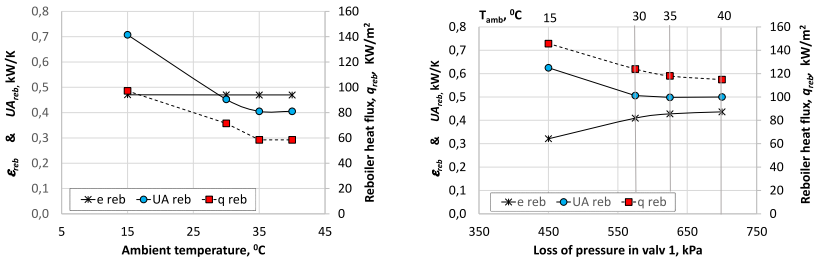


**Fig. 6.** Re-boiler: effectiveness, thermal conductance, and heat flux, in the a) reference and b) personalised configuration.

$$RR_{dc} = \frac{\dot{m}_{v\ in,dc} - \dot{m}_{v,out,dc}}{\dot{m}_{v,out,dc}},$$

which allows us to evaluate the vapour fraction that returns to the re-boiler. Similarly, in the rectifier, the reflux ratio, $RR_{rect}$, indicates the fraction of condensate from the vapour flow. It is evaluated as

$$RR_{rect} = \frac{\dot{m}_{v\ in,rect} - \dot{m}_{ref}}{\dot{m}_{ref}},$$

Table 5 shows how an increase in $\Delta P_{val\ 1}$ leads to a reduction in $OP_{dc}$ of 18.7% at $T_{amb} = 40$ °C, indicating that the operation of the column of distillation approaches the weeping mode. This mode is unsuitable because it impedes the interaction of liquid-vapour flows and hampers the purification of the vapour. The decrease in $OP_{dc}$ is caused by a decrease in $q_{reb}$, resulting in a decrease in the flow of vapour. In contrast, $OP_{dc}$ increases by 101.3% as $T_{cf,hot}$ increases by 50 °C, according to the behaviour of $q_{reb}$. On the other hand, Table 5 illustrates the contribution of the column of distillation to the vapour purification process. This contribution is evaluated by determining the increase in the ammonia mass fraction of the vapour flow, represented as $\Delta x_{dc}$. Note that an increase in $\Delta P_{val\ 1}$ results in a decrease in $\Delta x_{dc}$.

The SolutionCooled rectifier follows a similar trend; however, with a more pronounced impact, since there is a decrease of 70.6% in $\Delta x_{rect}$ due to increases in $P_H$. On the contrary, an inverse trend is observed in $\Delta x_{dc}$ when $T_{cf,\ hot}$, increases due to an increase in the water content in the vapour flow. Furthermore, it can be observed that $T_{cf,hot,}$ has a negligible effect on $\Delta x_{rect}$. However, neither $\Delta P_{val\ 1}$ nor $T_{cf,\ hot}$, significantly affect the refrigerant mass fraction, $x_{ref}$. However, a 75% increase in $\Delta P_{val\ 1}$ at $T_{amb} = 40$ °C in the personalised configuration leads to a notable increase of 68.6% in $RR_{rect}$.

The flow undergoes purification in the column of distillation at $T_{cf,\ hot} = 210$ °C, due to the absorption of ammonia from the downward liquid solution. This results in an increase in the mass of the vapour flow and negative $RR_{dc}$ values, even for a low $\Delta P_{val\ 1}$. However, when $T_{cf,\ hot} = 160$ °C, purification occurs by partial condensation of the water content of the vapour flow, leading to a reduction in mass [19]. Consequently, $RR_{dc}$ takes positive values. Table 5 illustrates that there is a 628.3% reduction in $\Delta RR_{dc}$ when $T_{cf,\ hot,}$ increases from 160 to 210 °C at $T_{amb} = 40$ °C. However, the impact of $\Delta P_{val\ 1}$ on $\Delta RR_{dc}$ is insignificant.

Regarding $T_{amb}$, it is shown in Fig. 7a that in the reference configuration, both $\Delta x_{rect}$ and $\Delta x_{dc}$ decrease as $T_{amb}$ increases. This trend is comparable to that observed when increasing $\Delta P_{val\ 1}$, although it is not as pronounced. It is worth noting that a $T_{amb}$ variation within the range of 15–40 °C results in an approximate 47% increase in $P_H$ (as shown in Fig. 4b) compared to the 75% increase in the personalised configuration. The illustration shows that $T_{amb}$ significantly affects the performance of the column of distillation, causing it to operate in weeping mode at a temperature of 35 °C or higher in the reference configuration. Furthermore, the findings display an increase in $RR_{rect}$ (Fig. 7b) consistent with the pattern observed with elevated $\Delta P_{val\ 1}$.

Analysis of the behaviour of the personalised configuration (Fig. 8a and b) shows that $\Delta x_{rect}$ is clearly lower compared to the reference configuration, decreasing as $T_{amb}$ increases. This behaviour is attributable to the growth of $\Delta P_{val\ 1}$. However, $\Delta x_{rect}$ reaches higher values due to $T_{cf,hot}$ growth. The rectification process in the column of distillation is due to the absorption of ammonia, as revealed by the negative values of $RR_{dc,}$ which reveals that $T_{cf,hot}$ and not $\Delta P_{val\ 1}$ is the parameter that governs the purification process in the column of distillation.

However, the column of distillation operates far from the weeping mode, despite the adverse effect of $\Delta P_{val\ 1}$, even at a temperature of 40 °C. The figure for $x_{ref}$ shows an increase as $T_{amb}$ increases, which is due to the increase in the coolant and liquid heat transfer coefficients, $h_{t\ cf}$, $h_{t\ L}$ (see Fig. 9a), as noted in Ref. [45]. In the personalised configuration (Fig. 9b), it behaves similarly due to the minimal influence of $\Delta P_{val\ 1}$ and $T_{cf,hot}$ on $x_{ref}$ and $h_{t\ cf}$.

**Table 5**
Purification system. Comparative results, expressed in %.

| $\Delta P_{val\ 1}$, kPa | $T_{cf,hot,}$ °C | $T_{amb,}$ °C | $\Delta OP_{dc}$ | $\Delta\Delta x_{dc}$ | $\Delta\Delta x_{rect}$ | $\Delta RR_{dc}$ | $\Delta RR_{rect}$ | $\Delta x_{ref}$ | $\Delta h_{t\ cf}$ |
|---|---|---|---|---|---|---|---|---|---|
| $\Delta P_{val\ 1L}$ vs. 175 | 210 | 30 | −13.8 | −16.6 | −60.4 | 0 | 67.2 | 0 | 0 |
| | | 40 | −18.7 | −13.7 | −70.6 | 0 | 68.6 | 0 | 0 |
| 175 | 210 vs. 160 | 30 | 65.1 | 63.0 | 5.8 | −287.3 | −9.7 | 0 | 0 |
| | | 40 | 101.3 | 68.9 | 13.4 | −628.3 | −20.0 | 0 | 0 |

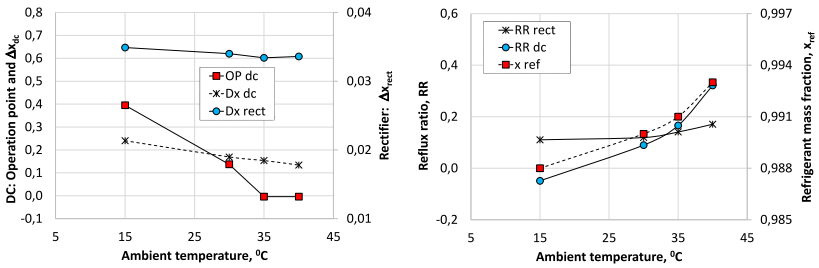


**Fig. 7.** Vapour purification system: a) operation point of the column of distillation, increase in the mass fraction of the vapour flow in the column of distillation, $\Delta x_{dc}$, and in the rectifier, $\Delta x_{rect}$, b) reflux ratio in the column of distillation, $RR_{dc}$, and in the rectifier, *RRrect* and the mass fraction of the refrigerant, $x_{ref}$, in the reference configuration.

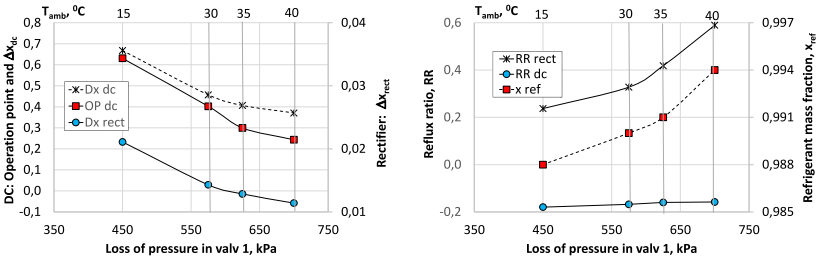


**Fig. 8.** Vapour purification system: a) operation point of the column of distillation and increase in mass fraction of the vapour flow in the column of distillation, $\Delta x_{dc}$, and in the rectifier, $\Delta x_{rect}$, b) reflux ratio in the column of distillation, $RR_{dc}$ and in the rectifier, $RR_{rect}$, and mass fraction of the refrigerant, $x_{ref}$, in the personalised configuration.

Finally, Fig. 10a shows the evolution of the temperature and vapour mass fraction on each column of distillation plate. The figure shows that the purification process of the vapour flow obtained in the re-boiler reached a plateau on the seventh plate, as reported by Ref. [46]. The plateau on a lower plate is reached when $T_{cf,hot}$ is 160 °C, which is aligned with the lower extension of the purification process in the column of distillation when $T_{cf\ hot}$ reduces. A similar pattern is observed when $\Delta P_{val\ 1}$ increases.

The graph in Fig. 10b shows the change in the mass fraction of the vapour flow in the rectifier, along with the corresponding temperature of the cooling solution in the column of distillation. Plate 2 refers to the plate located directly above the re-boiler. It is worth noting that the cooling solution experienced a significant initial temperature increase in the personalised setup at $T_{amb}$ of 30 and 40 °C, which is attributed to the substantial thermal gap generated between the cooling solution and the condensate caused by the elevated $P_H$ level reached.

The study suggests that when $\Delta P_{val\ 1}$ increases, the vapour purification process shifts from the column of distillation to the rectifier. As a result, the number of trays in the column of distillation decreases, and the reflux ratio in the rectifier rises. Moreover, the column of distillation may operate in weeping mode if $T_{cf\ hot}$ is not sufficiently elevated.

### 3.3. SolutionCooled absorber

Table 6 shows that the dilute solution entering the SolutionCooled absorber often transforms into a two-phase flow ($\Delta Q_{in\ cabs} = 100$) when it passes through the solution valve under increasing $\Delta P_{val\ 1}$ conditions. This transformation can impede the operation of the SolutionCooled absorber. On the contrary, when $T_{cf,hot}$ rises, the opposite trend occurs. At $T_{amb} = 40$ °C and according to Ref. [16], the

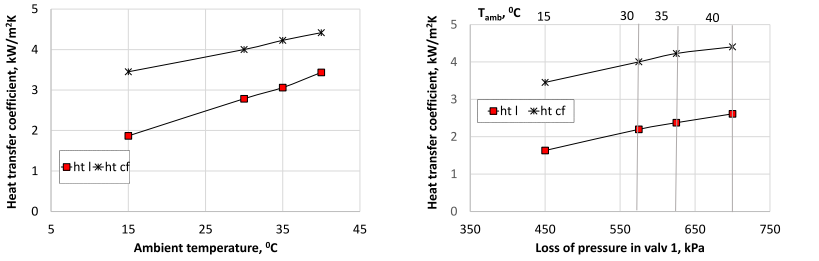


**Fig. 9.** Vapour purification system: coolant and liquid heat transfer coefficients, $h_{t\ cf}$, $h_{t\ l}$, in a) reference and b) personalised configuration.

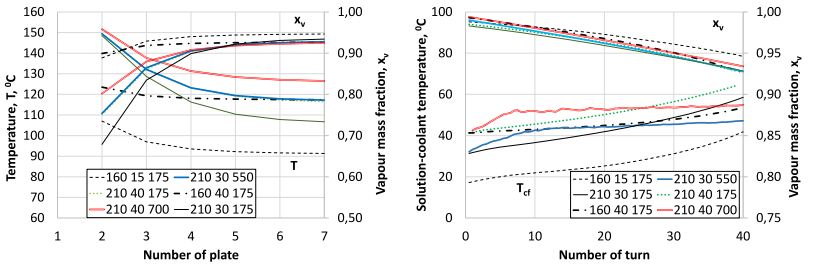


**Fig. 10.** Vapour purification system: a) temperature, $T$, and mass fraction, $x_v$, in the column of distillation, and b) mass fraction of the vapour, $x_v$, and temperature of the coolant solution, $T_{cf}$, in the rectifier. Box: feed hot water temperature and ambient temperature, °C; $\Delta P_{valv1}$, in kPa.

amount of absorbed refrigerant flow, $\Delta\dot{m}_{ref\ cabs}$, increases by 38.5% when $T_{cf,hot}$ rises from 160 to 210 °C in the SolutionCooled absorber. This is because the thermal gradient between the dilute solution flow and the solution-coolant flow is favoured, thereby facilitating the rejection of the absorption heat. As a result, the efficiency of the SolutionCooled absorber, $\varepsilon_{cabs}$, increases.

Furthermore, Fig. 11 illustrates that when $T_{cf,hot}$ reaches 210 °C, achieving the temperature difference at the pinch point value may postpone the start of the absorption process, particularly at $T_{amb} = 40$ °C, which acts as a threshold in the SolutionCooled absorber. Then again, a high value of $\Delta P_{val1}$ could improve the absorption of the vapour, as long as it is possible to reduce the temperature of the dilute solution at the inlet of the SolutionCooled absorber, provided that it is reduced below the saturation temperature.

Concerning $T_{amb}$, Fig. 12a demonstrates that in the reference configuration, as $T_{amb}$ increases, the solution at the inlet of the SolutionCooled absorber changes to a two-phase flow, which adversely affects the operation of the refrigeration system. Additionally, $\Delta\dot{m}_{ref\ cabs}$ decreases because of the challenges of heat rejection during absorption as the $T_{amb}$ increases. Based on the above, Fig. 12b shows that $\Delta\dot{m}_{ref\ cabs}$ achieves a higher value in the personalised configuration in comparison to the reference configuration due to $T_{cf\ hot}$, which is higher in the latter, although it is somewhat mitigated by the rise in $T_{amb}$ and in $\Delta P_{val1}$.

The findings indicate that there is a maximum increase in $\Delta P_{val\ 1}$ due to the promotion of a two-phase change in the flow of the dilute solution. A similar effect is seen with an increase in $T_{amb}$. Furthermore, unlike ambient temperature, $\Delta P_{val\ 1}$ can be controlled. In this way, $\Delta P_{val\ 1}$ could be selected to increase the absorption of refrigerant vapour in the SolutionCooled absorber, thus optimising COP. To achieve this, the temperature drop in the dilute solution resulting from the heat recovered in the generator assembly plus that caused by the $\Delta P_{val1}$ should be chosen so that the temperature of the dilute solution entering the SolutionCooled absorber is at least below the saturation temperature.

### 3.4. Internal heat recovery and exergy destruction

Table 7 illustrates that as $T_{cf,hot}$ increases, the contribution of the generator heat recovery system to the internal heat recovery of the refrigeration system also increases. Internal heat recovered by the SolutionCooled absorber follows a similar pattern, as indicated in Ref. [47]. Furthermore, the results suggest that the contribution of the generator to internal heat recovery is predominant when $\Delta P_{val1}$ increases, shifting the balance in favour of the generator over the SolutionCooled absorber. This phenomenon is consistent with the observation that the temperature overlap decreases in the SolutionCooled absorber (see Fig. 11) as the thermal lift increases.

Regarding the temperature of the environment, it can be observed in Fig. 13a that there is an increase in the heat recovered from both the generator and the absorber when $T_{amb}$ increases. This trend is also observed when the variable $\Delta P_{val\ 1}$ increases. Fig. 13b shows the internal thermal load in the personalised configuration. In this configuration, the temperature overlap in the SolutionCooled absorber undergoes only minor changes, since the effect of the increase in the temperature of the cold fluid is counteracted by the increase in the $\Delta P_{val\ 1}$ variable. Therefore, the thermal load of the SolutionCooled absorber is similar in both configurations. There are no significant discrepancies in the thermal load of the refrigeration heat exchanger. Comparison of the personalised configuration with the reference configuration reveals the most significant alterations in the internal thermal load of the generator heat recovery and the rectifier. It should be noted that the thermal load of both components decreases as a result of the reduced $T_{cf,hot}$, as shown in the figure.

Table 8 shows that the contribution of the heat recovery loop, consisting of a column of distillation, rectifier, SolutionCooled absorber, solution pump, solution valve, and re-boiler, to the total exergy destruction of the refrigeration system increases slightly by 2.7 % as $\Delta P_{val\ 1}$ raises from 175 kPa to $\Delta P_{val\ 1L}$, at $T_{cf,hot} = 210$ °C and $T_{amb} = 40$ °C. This happens because the contribution of the purification system increases at the expense of that of the re-boiler and the SolutionCooled absorber, which increase its thermal load. On the other hand, the table shows that the contribution of the heat recovery loop is reduced in favour of the other components of the refrigeration system when $T_{cf,hot}$ rises. Nevertheless, the re-boiler increases its contribution. Note that the exergy efficiency of the system experiences a slight reduction. Jiménez-García et al. [48] also reported this trend.

Regarding $T_{amb}$, Fig. 14a shows that the contribution of the heat recovery loop to the total exergy destruction in the system is approximately 70 % in the reference configuration, increasing at $T_{amb} = 40$ °C. The figure also shows that the SolutionCooled absorber is the largest contributor, closely followed by the re-boiler. However, the contribution of internal heat recovery in the generator to total exergy destruction increases as $T_{amb}$ increases, at the expense of the other components of the heat recovery loop. This behaviour is consistent with that observed as $\Delta P_{val\ 1}$ increases.

However, Fig. 14b illustrates that the contribution of the heat recovery loop is reduced in the personalised configuration,

**Table 6**
Comparative results in the SolutionCooled absorber (%).

| $\Delta P_{val\ 1}$, kPa | $T_{cf,hot,}$ °C | $T_{amb}$, °C | $\Delta Q_{in\ cabs}$ | $\Delta\Delta\dot{m}_{ref\ cabs}$ | $\Delta\varepsilon_{cabs}$ |
|---|---|---|---|---|---|
| $\Delta P_{val\ 1L}$ vs. 175 | 210 | 30 | 100 | −11.5 | 0 |
| | | 40 | 62.5 | −21.3 | 0 |
| 175 | 210 vs. 160 | 30 | −100 | 10.8 | 0.7 |
| | | 40 | −59.0 | 38.5 | 4.2 |

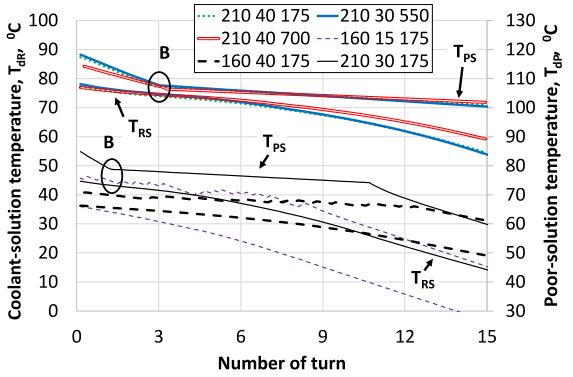


**Fig. 11.** SolutionCooled absorber: evolution of the temperature of the dilute and coolant solution, $T_{dP}$, $T_{dR}$, respectively. Rectangle: feed hot water temperature, outdoor temperature, °C; and $\Delta P_{valv1}$, kPa. Pinch point: B.

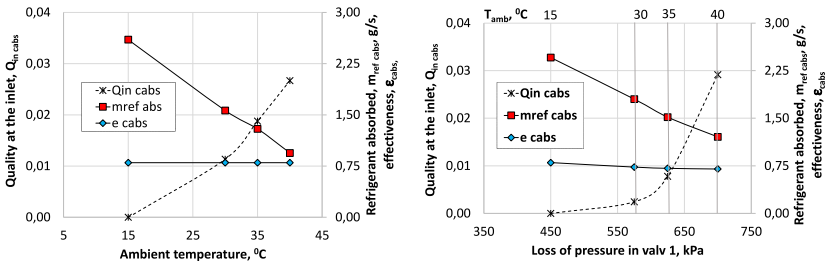


**Fig. 12.** SolutionCooled absorber: quality of the dilute solution at the inlet, absorbed refrigerant flow, and effectiveness, in a) reference and b) personalised configuration.

**Table 7**
Comparative results in the internal heat recovery: contribution of the column of distillation plus the solution heat exchanger and the SolutionCooled absorber (%).

| $\Delta P_{val\ 1}$, kPa | $T_{cf,hot,}$ °C | $T_{amb}$, °C | $\Delta Q_{dc\ +\ SHX}$ | $\Delta Q_{cabs}$ |
|---|---|---|---|---|
| $\Delta P_{val\ 1L}$ vs. 175 | 210 | 30 | 5.3 | −4.7 |
| | | 40 | 6.1 | −15.3 |
| 175 | 210 vs. 160 | 30 | 10.9 | 12.5 |
| | | 40 | 12.0 | 16.4 |

attributable to the increase in $T_{cf,hot}$, partially overcome by the increase in the generator contribution at high $T_{amb.}$ Furthermore, the amount of exergy destroyed in the personalised configuration increases compared to the reference configuration, as reported in Ref. [49] due to the higher cooling capacity of the former. Finally, the exergy efficiency of the system barely decreases, which is mainly attributed to the other components of the refrigeration system, not to the components analysed in this work.

## 4. Conclusions

In this study, an extensive analysis was carried out on the functional performance of the commercial Robur refrigeration absorption machine (ACF60-00 LB). The chiller uses a single effect $NH_3/H_2O$ system, which is indirectly AirCooled and hot water powered mainly for refrigeration purposes. In particular, the refrigeration unit employs a modified GAX cycle, which provides different features.

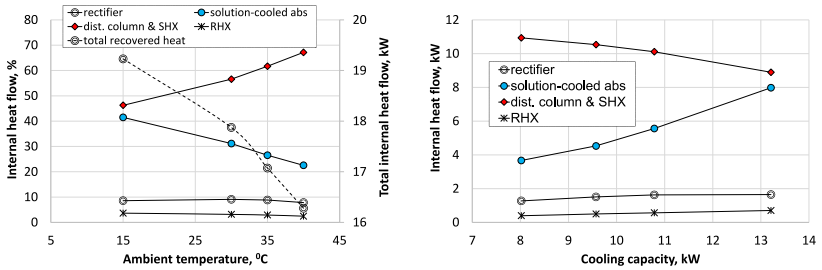


**Fig. 13.** a) Contribution to internal heat recovery: rectifier, column of distillation, SolutionCooled absorber, solution heat exchanger, refrigeration heat exchanger, %, and total internal heat recovered, kW, in the reference configuration. b) Internal heat recovery in the personalised configuration. Internal heat flow in generator and rectifier in the reference configuration, in dashed line.

**Table 8**
Contribution to exergy destruction: rectifier, re-boiler, column of distillation, SolutionCooled absorber, and heat recovery system of the refrigeration machine. Exergy efficiency. The comparative results are expressed as (%).

| $\Delta P_{val\ 1}$, kPa | $T_{cf,hot,}$ °C | $T_{amb,}$ °C | $\Delta I_{rect}$ | $\Delta I_{reb}$ | $\Delta I_{dc+SHX}$ | $\Delta I_{cabs}$ | $\Delta I_{\text{sol loop}}$ | $\Delta\eta_{ex}$ |
|---|---|---|---|---|---|---|---|---|
| $\Delta P_{val\ 1L}$ vs. 175 | 210 | 30 | 18.1 | −9.9 | 14.9 | −12.9 | 2.2 | −8.0 |
| | | 40 | 12.2 | −11.7 | 26.9 | −19.4 | 2.7 | −7.4 |
| 175 | 210 vs. 160 | 30 | −25.9 | 13.4 | −18.1 | −39.3 | −13.4 | −6.9 |
| | | 40 | −27.6 | 28.4 | −38.3 | −34.9 | −20.2 | −7.9 |

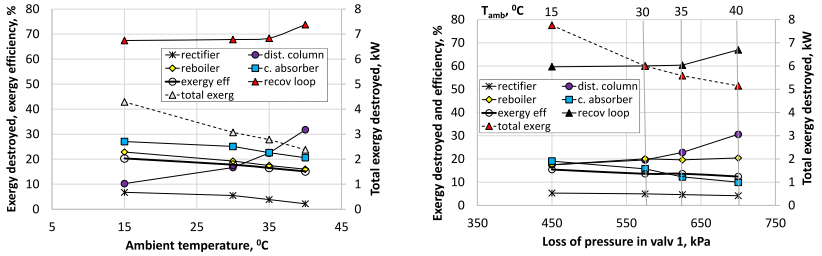


**Fig. 14.** Contribution to exergy destruction: refrigerator, column of distillation, rectifier, SolutionCooled absorber and heat recovery loop (%), total exergy destruction in the system (kW) and exergy efficiency (%) in a) reference and b) personalised configuration.

Furthermore, the refrigeration unit integrates an additional valve is integrated into the system, which provides an interesting opportunity to adjust the high pressure level and study the effect on the internal heat recovery capacity. The main objective of this research study is to analyse the capacity of the refrigeration system to recover internal heat to improve its overall performance.

A differential mathematical model, including species, mass, and energy balance, is used to achieve the goal. The model uses heat and mass transfer coefficients evaluated locally and operates on a modular structure. The results have been verified against data provided by the manufacturer and published in the literature.

The numerical results indicate that $T_{cf,hot}$ primarily governs the re-boiler heat flow, which increases proportionally to $T_{cf,hot}$. However, the increase in $\Delta P_{val\ 1}$ partially overshadows the re-boiler heat flow, especially at high $T_{amb}$. With respect to the purification system, the results reveal a decrease in the extension of the vapour purification process in the column of distillation, particularly in the rectifier. Furthermore, the negative impact caused by the increase that $\Delta P_{val\ 1}$ on the risk of the column of distillation operates in weeping mode is considerably reduced at elevated $T_{cf,hot}$. The findings indicate that $\Delta P_{val1}$ has a negligible impact on the mass fraction of the refrigerant flow.

The findings of the SolutionCooled absorber suggest that the diluted solution at the inlet tends to become a two-phase flow when $\Delta P_{val\ 1}$ increases, which is an unfavourable result. Additionally, the amount of refrigerant absorbed in the SolutionCooled absorber is reduced. However, enlargement in $\Delta P_{val\ 1}$ could improve refrigerant absorption, mainly at elevated ambient temperatures. On the contrary, the contribution of the SolutionCooled absorber to internal heat recovery is prioritised to the generator when there is an increase in $\Delta P_{val\ 1}$ at high $T_{cf,hot}$. Furthermore, the simulation demonstrates that internal heat recovery in the generator has an increased contribution to total exergy destruction, at the cost of other components in the heat recovery loop. These changes are evident in the corresponding exergy destruction behaviour.

Specifically, the findings indicate that when the value of $\Delta P_{val\ 1}$ increases by 75% at $T_{cf,hot} = 210$ °C and $T_{amb} = 40$ °C:

- The re-boiler heat flow decreases by 8.4% and consequently reduces the cooling capacity of the system.

- Despite the reduced cooling capacity, there is no risk that the column of distillation will operate in weeping mode.
- The extension of the vapour purification process decreases by 13.7% in the column of distillation and by 70.6% in the rectifier.
- The refrigerant flow absorbed by the SolutionCooled absorber decreases by 21.3%.
- The internal thermal load of the generator assembly increases by 26.9%, while the capacity of the SolutionCooled absorber is reduced by 19.4%.
- The appearance of a two-phase solution flow at the inlet of the SolutionCooled absorber adversely affects the operation of the SolutionCooled absorber.
- The contribution of the heat recovery loop to the total exergy destruction of the refrigeration system increases slightly by 2.7% due to the contribution of the vapour purification system increasing at the expense of that of the re-boiler and the SolutionCooled absorber.

This study demonstrates to what extent the modified GAX-based cycle can operate efficiently at high thermal lifts, resulting in a high COP refrigeration system. When the absorption chiller operates under such conditions, the findings show that elevated $\Delta P_{val1}$ leads to an increase in the internal thermal load of the generator. Furthermore, the purification process is sifted from the column of distillation to the rectifier, reducing its number of plates. Additionally, there is a potential risk of two-phase flow at the inlet of the SolutionCooled absorber when the feed water temperature is not sufficiently high, which would deteriorate the COP of the chiller. However, the contribution of the internal heat recovery system to the total exergy destruction of the refrigeration system is not particularly significant. Finally, the opportunity to optimise COP by controlling $\Delta P_{val1}$ is presented.

## Statement on data availability

Data will be made available upon request.

## Additional information

No additional information is available for this paper.

## CRediT authorship contribution statement

**María Esther Palacios-Lorenzo:** Writing – review & editing, Writing – original draft, Visualization, Validation, Supervision, Software, Methodology, Investigation, Formal analysis, Data curation, Conceptualization. **José Daniel Marcos:** Writing – review & editing, Resources, Project administration, Methodology, Conceptualization.

## Declaration of competing interest

The authors declare that they have no known competing financial interests or personal relationships that could have appeared to influence the work reported in this paper.

## Acknowledgement

The research is funded by the Horizon 2020 Research and Innovation Programme of the European Union within the framework of the ASTEP project under grant agreement No. 88441 and the 2018 Regional Research and Technology Development Programme within the framework of the ACES2030CM project (Ref P2018/EMT-4319).

## Abbreviations

*Symbols*

| | |
|---|---|
| $A$ | transfer area, $m^2$ |
| $A_a$ | tray active area, $m^2$ |
| $A_d$ | downcomer area, $m^2$ |
| $A_h$ | tray hole area, $m^2$ |
| $A_h/A_t$ | fractional free area |
| $A_t$ | cross-sectional area, $m^2$ |
| $d_h$ | tray hole diameter, m |
| $e$ | wall thickness, m |
| $e_{tray}$ | spacing tray, m |
| $e_M$ | Murphree efficiency |
| $f$ | circulation ratio, $\dot{m}_{dR}/\dot{m}_{ref}$ |
| $h_f$ | re-boiler length, m |
| $h$ | specific enthalpy, $kJ \bullet kg^{-1}$ |

| | |
|---|---|
| $h_f$ | fin length, m |
| $h_m$ | mass transfer coefficient |
| $h_t$ | heat transfer coefficient, $W \bullet m^{-2} \bullet K^{-2}$ |
| $\widetilde{h}$ | partial enthalpy, $J \bullet kg^{-1}$ |
| $\dot{m}$ | mass flux. $Kg \bullet s^{-1}$ |
| $P$ | pressure, Pa |
| $Q_{in\ cabs}$ | quality of the dilute solution flow at the SolutionCooled absorber inlet |
| $\dot{Q}$ | heat flow, W |
| $q$ | heat flux, $W \bullet m^{-2}$ |
| $s$ | pitch of the fin, m |
| $T$ | temperature, °C |
| $t_m$ | thickness of the fin, m |
| $UA$ | thermal conductance, $W \cdot K^{-1}$ |
| $x$ | ammonia mass fraction, kg $NH_3 \bullet kmol^{-1}$ |
| $\overline{x}$ | ammonia molar fraction, kmol $NH_3 \bullet kmol^{-1}$ |
| $z$ | ratio of ammonia to the total molar flux across the vapour-liquid interface |

*Subscripts and superscripts*

| | |
|---|---|
| abs | AirCooled absorber |
| air | coolant air |
| cabs | SolutionCooled absorber |
| cond | AirCooled condenser |
| cf | coupling fluid |
| dP | dilute solution in ammonia |
| dR | concentrate solution in ammonia |
| e | in thermodynamic equilibrium |
| evap | evaporator |
| reb | re-boiler |
| rect | SolutionCooled rectifier |
| ref | refrigerant |

## References


[1] IEA, Energy technology perspectives, in: Energy Technology Perspectives 2023 – Analysis - IEA, 2023.
[2] The Role of the Refrigeration in the Global Economy, 38th Informatory Note on Refrigeration Technologies, International Institute of Refrigeration, 2019. https://iifir.org/en/fridoc/the-role-of-refrigeration-in-the-global-economy-2019-142028.
[3] D. Keppler, Absorption chillers as a contribution to a climate-friendly refrigeration supply regime: factors of influence on their further diffusion, J. Clean. Prod. 172 (2018) 1535–1544, https://doi.org/10.1016/j.jclepro.2017.10.276.
[4] R. Nikbakhti, X. Wang, A.K. Hussein, A. Iranmanesh, Absorption cooling systems – review of various techniques for energy performance enhancement, Alex. Eng. J. 59 (2020) 707–738, https://doi.org/10.1016/j.aej.2020.01.036.
[5] A. Altamirano, N. Pierrès, B. Stutz, Review of small-capacity single-stage continuous absorption systems operating on binary working fluids for cooling: theoretical, experimental and commercial cycles, Int. J. Refrig. 106 (2019) 350–373, https://doi.org/10.1016/j.ijrefrig.2019.06.033.
[6] W. Wu, B. Wang, W. Shi, X. Li, An overview of ammonia-based absorption chillers and heat pumps, Renewable Sustainable Energy Rev. 31 (2014) 681–707, https://doi.org/10.1016/j.rser.2013.12.021.
[7] J. Fernández-Seara, J. Sieres, The importance of the ammonia purification process in ammonia–water absorption systems, Energy Convers. Manag. 47 (2006) 1975–1987. https://doi:10.1016/j.enconman.2005.09.002.
[8] S. Malaine, N. Ababssi, M. Charia, A. Boulal, Enhancing benefits by rectification in the absorption refrigeration systems, Int. J. Therm. 25 (2022) 29–37. https://doi:10.5541/ijot.927046.
[9] J. Sieres, J. Fernandez-Seara, Evaluation of the column components size on the vapour enrichment and system performance in small power NH3–H2O absorption refrigeration machines, Int. J. Refrig. 9 (2006) 579–588. https://doi:10.1016/j.ijrefrig.2005.10.004.
[10] A.M. Abed, M.A. Alghoul, K. Sopian, H. Sh Majdi, A.N. Al-Shamani, A.F. Muftah, Enhancement aspects of single stage absorption cooling cycle: a detailed review, Renewable Sustainable Energy Rev. 77 (2017) 1010–1045, https://doi.org/10.1016/j.rser.2016.11.231.
[11] Y.T. Kang, Y. Kunugi, T. Kashiwagi, Review of advanced absorption cycles: performance improvement and temperature lift enhancement, Int. J. Refrig. 23 (2000) 388–401, https://doi.org/10.1016/S0140-7007(99)00064-X.
[12] C.P. Jawahar, R. Saravanan, Generator absorber heat exchange-based absorption cycle-A review, Renewable Sustainable Energy Rev. 14 (2010) 2372–2382, https://doi.org/10.1016/j.rser.2010.05.002.
[13] N. Velázquez, R. Best, Methodology for the energy analysis of an air-cooled GAX absorption heat pump operated by natural gas and solar energy, Appl. Therm. Eng. 22 (2002) 1089–1103, https://doi.org/10.1016/S1359-4311(02)00028-5.
[14] V.H. Gómez, A. Vidal, R. Best, O. Garcia-Valladares, N. Velázquez, Theoretical and experimental evaluation of an indirect-fired GAX cycle cooling system, Appl. Therm. Eng. 28 (2008) 975–987, https://doi.org/10.1016/j.applthermaleng.2007.06.027.
[15] M.A. Siddiqui Saghiruddin, Economic analyses and performance study of three ammonia-absorption cycles using heat recovery absorber, Energy Convers. Manag. 37 (1996) 421–432, https://doi.org/10.1016/0196-8904(95)00204-9.
[16] S. Du, R.Z. Wang, Z.Z. Xia, Optimal ammonia water absorption refrigeration cycle with maximum internal heat recovery derived from pinch technology, Energy 68 (2014) 862–869, https://doi.org/10.1016/j.energy.2014.02.065.
[17] E. Dai, T. Jia, Y. Dai, Theoretical and experimental investigation on a GAX-Based NH3-H2O absorption heat pump driven by parabolic trough solar collector, Sol. Energy 197 (2020) 498–510, https://doi.org/10.1016/j.solener.2020.01.011.

[18] C.P. Jawahar, R. Saravanan, Experimental studies on air-cooled $NH_3$-$H_2O$ based modified GAX absorption cooling system, Int. J. Refrig. 34 (2011) 658–666, https://doi.org/10.1016/j.ijrefrig.2010.11.005.
[19] M. Aprile, R. Scoccia, T. Toppi, M. Guerra, M. Motta, Modelling and experimental analysis of a GAX NH3–H2O gas-driven absorption heat pump, Int. J. Refrig. 66 (2016) 145–155, https://doi.org/10.1016/j.ijrefrig.2016.02.008.
[20] J. Fernández-Seara, F.J. Uhía, J. Sieres, Analysis of an air-cooled ammonia–water vertical tubular absorber, Int. J. Therm. Sci. 46 (2007) 93–103, https://doi.org/10.1016/j.ijthermalsci.2006.03.005.
[21] A.M. Blanco-Marigorta, J.D. Marcos, Key issue on the exergy analysis of $H_2O$/LiBr absorption cooling systems, Case Stud. Therm. Eng. 28 (2021) 101568, https://doi.org/10.1016/j.csite.2021.101568.
[22] A.K. Coker, Ludwing's Applied Process Design for Chemical and Petrochemical Plants, 4, Elsevier, 2010, https://doi.org/10.1016/B978-0-7506-7766-0.X5000-3.
[23] O.M. Ibrahim, S.A. Klein, Thermodynamic Properties of Ammonia-Water Mixtures, ASHRAE Transactions, 1993, pp. 1495–1502. Symposia. (PDF) Thermodynamic properties of ammonia-water mixtures (researchgate .net).
[24] R.M. Lazzarin, A. Gasparella, G.A. Longo, Ammonia-water absorption chiller for refrigeration: theoretical and real performances, Int. J. Refrig. 19 (1996) 239–246, https://doi.org/10.1016/0140-7007(96)00016-3.
[25] G. Grossman, A. Zaltash, ABSIM- modular simulation of advanced absorption systems, Int. J. Refrig. 24 (2001) 531–543, https://doi.org/10.1016/S0140-7007(00)00051-7.
[26] F. Táboas, M. Vallès, M. Bourouis, A. Coronas, Pool boiling of ammonia/water and its pure components: comparison of experimental data in the literature with the predictions of standard correlations, Int. J. Refrig. 30 (2007) 778–788, https://doi.org/10.1016/j.ijrefrig.2006.12.009.
[27] J. Sieres, J. Fernández-Seara, Modelling of simultaneous heat and mass transfer processes in ammonia-water absorption systems from general correlations, Heat Mass Tran. 44 (2007) 113–123, https://doi.org/10.1007/s00231-006-0226-3.
[28] T. Morosuk, G. Tsatsaronis, A new approach to the exergy analysis of absorption refrigerant machines, Energy 33 (2008) 890–907, https://doi.org/10.1016/j.energy.2007.09.012.
[29] D. Barnea, A unified model for prediction flow-pattern transition from the whole range of pipe inclinations, Int. J. Multiphas. Flow 13 (1987) 1–12, https://doi.org/10.1016/0301-9322(87)90002-4.
[30] L. Yi-ping, Z. Hua, W. Shu-hua, W. Jing, Gas–liquid interfacial friction factor for the transition from stratified to slug flow, Microgravity Sci. Technol. 20 (2008) 299–305, https://doi.org/10.1007/s12217-008-9078-4.
[31] R.N. Hassanlouei, H. Firouzfar, N. Kasiri, M.H. Khanof, A simple mathematical model for slug liquid holdup in horizontal pipes, Sci. Iran. C 19 (2012) 1653–1660, https://doi.org/10.1016/j.scient.2012.05.010.
[32] P.L. Spedding, N.P. Hand, Prediction in stratified gas-liquid co-current flow in horizontal pipelines, Int. J. Heat Mass Tran. 40 (1997) 1923–1935, https://doi.org/10.1016/S0017-9310(96)00252-9.
[33] D. Barnea, N. Brauner, Holdup of the liquid slug in two phase intermittent flow, Int. J. Multiphas. Flow 11 (1985) 43–49, https://doi.org/10.1016/0301-9322(85)90004-7.
[34] F.A. Franca, A.C. Bannwart, R.M.T. Camargo, M.A.L. Gonçalves, Mechanistic modelling of the convective heat transfer coefficient in gas-liquid intermittent flows, Heat Tran. Eng. 29 (2008) 984–998, https://doi.org/10.1080/01457630802241091.
[35] E. Al-Safran, Investigation and prediction of slug frequency in gas/liquid horizontal pipe flow, J. Petrol. Sci. Eng. 69 (2009) 143–155, https://doi.org/10.1016/j.petrol.2009.08.009.
[36] D. He, S. Chen, B. Bai, Void fraction measurement of stratified gas-liquid flow based on multi-wire capacitance probe, Exp. Therm. Fluid Sci. 102 (2019) 61–73, https://doi.org/10.1016/j.expthermflusci.2018.11.005.
[37] A.F. Mills, Transferencia de Calor, McGrawHill, 4th ed., 2011. ISBN: 978-0-07-339812-9.
[38] F. Táboas, M. Vallès, M. Bourouis, A. Coronas, Pool boiling of ammonia/water and its pure components: comparison of experimental data in the literature with the predictions of standard correlations, Int. J. Refrig. 30 (2007) 778–788, https://doi.org/10.1016/j.ijrefrig.2006.12.009.
[39] V.D.I. Wärmeatlas, VDI Heat Atlas, 2nd ed., Springer, 2010. ISBN: 9783540778769/9783540778776.
[40] N.A.A. Qasem, S.M. Zubair, Compact and microchannel heat exchangers: a comprehensive review of airside friction factor and heat transfer correlations, Energy Convers. Manag. 173 (2008) 555–601, https://doi.org/10.1016/j.enconman.2018.06.104.
[41] D.S. Scott, W. Hayduk, Gas absorption in horizontal cocurrent bubble flow, Can. J. Chem. Eng. (1996) 130–136, https://doi.org/10.1002/cjce.5450440302.
[42] J.W. Ciborowski, R.M. Rychlicki, Mass transfer in two-phase gas-liquid wavy flow, Int. J. Heat Mass Tran. (1971) 1261–1274, https://doi.org/10.1016/0017-9310(71)90176-1.
[43] J.J. Pereira, C.A. Cabral, C. Almir, J.B. Furlan, A. Ochoa, C. Dutra, Energetic analysis of a commercial absorption refrigeration unit using an ammonia-water mixture, Acta Sci. Technol. 39 (2017) 439–448, https://doi.org/10.4025/actascitechnol.v39i4.29904.
[44] S. Klein, A Model of the Steady-State Performance of an Absorption Heat Pump, US Department of Commerce, 1992. QC 100.U56 82-2602. A model of the steady-state performance of an absorption heat pump : Klein, S. A. : Free Download, Borrow, and Streaming : Internet Archive.
[45] J. Fernández-Seara, J. Sieres, M. Vázquez, Heat and mass transfer analysis of a helical coil rectifier in an ammonia–water absorption system, Int. J. Therm. Sci. 42 (2003) 783–794, https://doi.org/10.1016/S1290-0729(03)00051-6.
[46] E.W. Zavaleta-Aguilar, J.R. Simões-Moreira, Thermal design of a tray-type column of distillation of an ammonia/water absorption refrigeration cycle, Appl. Therm. Eng. 41 (2012) 52–60, https://doi.org/10.1016/j.applthermaleng.2011.12.009.
[47] V.H. Gómez, A. Vidal, R. Best, O. García-Valladares, N. Velázquez, Theoretical and experimental evaluation of an indirect-fired GAX cycle cooling system, Appl. Therm. Eng. 28 (2008) 975–987, https://doi.org/10.1016/j.applthermaleng.2007.06.027.
[48] J.C. Jiménez-García, W. Rivera, Exergy analysis of an experimental ammonia/water absorption cooling system, Case Stud. Therm. Eng. 49 (2023) 103167, https://doi.org/10.1016/j.csite.2023.103167.
[49] G. Moreno-Quintanar, V. Gomez, R. Best, Exergetic analysis of a GAX refrigeration system design to operate with LP gas and solar energy, Energy Proc. 70 (2015) 644–651, https://doi.org/10.1016/j.egypro.2015.02.172.